Doppler broadening thermometry of acetylene and accurate measurement of the Boltzmann constant

R. Hashemi, C. Povey, M. Derksen, H. Naseri, J. Garber, and A. Predoi-Cross

Citation: The Journal of Chemical Physics **141**, 214201 (2014); doi: 10.1063/1.4902076
View online: http://dx.doi.org/10.1063/1.4902076
View Table of Contents: http://scitation.aip.org/content/aip/journal/jcp/141/21?ver=pdfcov
Published by the AIP Publishing

Doppler broadening thermometry of acetylene and accurate measurement of the Boltzmann constant

R. Hashemi, C. Povey, M. Derksen, H. Naseri, J. Garber, and A. Predoi-Cross[a)]
Alberta Terrestrial Imaging Centre, Department of Physics and Astronomy, University of Lethbridge, 4401 University Drive, Lethbridge, Alberta T1K3M4, Canada

(Received 10 May 2014; accepted 6 November 2014; published online 1 December 2014)

In this paper, we present accurate measurements of the fundamental Boltzmann constant based on a line-shape analysis of acetylene spectra in the $\nu_1 + \nu_3$ band recorded using a tunable diode laser. Experimental spectra recorded at low pressures (0.25 − 9 Torr), have been analyzed using a Speed Dependent Voigt model that takes into account the molecular speed dependence effects. This line-shape model reproduces the experimental data with good accuracy and allows us to determine precise line-shape parameters for the $P(25)$ transition of the $\nu_1 + \nu_3$ band. From the recorded spectra we obtained the Doppler-width and then determined the Boltzmann constant, k_B. © *2014 AIP Publishing LLC*. [http://dx.doi.org/10.1063/1.4902076]

I. INTRODUCTION

Acetylene is an important trace constituent in the atmospheres of Earth and other planets, and Saturn's Titan. This molecule is a light, linear molecule. Therefore, its spectrum is often straightforward to analyse. The $\nu_1 + \nu_3$ band of acetylene, with ν_1 as the symmetric CH stretch and ν_3 as the antisymmetric stretch is a strong absorption band compared to other nearby absorption bands. Therefore, it provides a good test case for measurements of fundamental physical constants such as the optical determination of the Boltzmann constant.

The motivation for this study is the retrieval of the Boltzmann constant (k_B) with high precision. The accepted value for the k_B published by the Committee on Data for Science and Technology (CODATA) is $1.3806488 \times 10^{-23}$ J K^{-1} with a relative uncertainty of 9.1×10^{-7}.[1] This value was determined based upon a number of studies described and referenced by Mohr *et al.*[1] using measurements of the ideal gas constant, R. The Boltzmann constant can be defined as $k_B = R/N_A$ where R is the ideal gas constant and N_A is Avogadro number. Thus, k_B can be calculated based upon an accurate determination of R.

One of the recent methods of measuring k_B is the laser spectroscopy using Doppler-width thermometry approach, which was used in our study. This alternate method has been attempted by different experimental groups and the calculated relative uncertainty in its value is of an order of 10^{-4} and 10^{-5}.[2–6] It is desirable to improve the known value of k_B to have relative accuracy higher than 10^{-6}. To achieve such a high accuracy, a significant improvement of the experimental precision is required.

The experiment is based on measuring ro-vibrational absorption features of C_2H_2 gas inside a temperature and pressure controlled cell maintained at thermal equilibrium. The width at half-maximum of the absorption line is dominated by the Doppler width due to the molecular velocity distribution along the laser beam at low gas pressure.

The Doppler width of a spectral absorption line recorded in a cell is related to the equilibrium temperature and Boltzmann constant as it is shown in Eq. (1)

$$k_B = \left(\frac{\gamma_D}{\nu}\right)^2 \left(\frac{Mc^2}{2\ln(2)T}\right), \quad (1)$$

where γ_D is the Doppler broadening, M is the mass of the gas particle, c is the speed of light, T is temperature, and ν is the line position.

Several research groups have carried out spectroscopic measurements to obtain k_B. Lemarchand *et al.*[7,8] have studied laser absorption spectroscopy in the mid-IR and corrected for the deviation resulting from the hyperfine structure and determined a value of $1.38080(20) \times 10^{23}$ J K^{-1} for k_B, which agreed within total systematic uncertainty about 2.3×10^{-6} to the accepted CODATA value which is a remarkable result. Casa *et al.*[3] have studied spectra of carbon dioxide transitions and have achieved an relative error of 1.6×10^{-4} in their reported value for k_B of $1.38058(13) \times 10^{-23}$ J K^{-1}. Yamada *et al.*[4] have determined k_B using the Doppler width of acetylene transitions and reported a value for the k_B equal to $1.3940(17) \times 10^{-23}$ J K^{-1}. This group mentioned that in their determination of the Doppler width of a ro-vibrational absorption line using a comb-locked diode laser the lack of accuracy in temperature measurement is the main contributor to the quoted error. Truong *et al.*[9] have measured k_B to be $1.38104(59) \times 10^{-23}$ J K^{-1}. The relative deviation of their result from CODATA value was 2.7×10^{-4}.

Cygan *et al.*[10] concluded that the line-shape models used in a line-shape study can influence the accuracy of Doppler widths retrieved by laser spectroscopy.

The common profiles used by the authors to analyse the spectra recorded at very low pressure were the Voigt profile (VP)[11] and the Gaussian profile. The influence of Dicke narrowing[12] on the accuracy of Doppler width measurements has been considered in several studies. Lemarchand *et al.*[7] have employed NH_3 spectra using the VP and Galatry (soft collisions)[13] models and they obtained k_B with an uncertainty

a)Electronic mail: Adriana.predoicross@uleth.ca.

as low as 3.7×10^{-5}. Recently, Castrillo *et al.*[14] have found the relative uncertainty of k_B to be 2.4×10^{-5} by using a line-shape study of H_2O and considering both the Speed Dependent Voigt (SDV) model[15–17] and the newly introduced partially correlated Speed Dependent Hard Collision (pcSDHC) profile.[18–20]

In this study, we used a 3-channel tunable diode laser spectrometer provided with a temperature and pressure-controlled cell to record spectra of the $P(25)$ line of acetylene. From these spectra, we measured the Doppler broadening of the $P(25)$ transition and retrieved the k_B using the SDV line-shape model. We compared our value of k_B with previous published results and the value reported in the CODATA database.

II. THEORETICAL LINE-SHAPE MODELS

Proper use of line-shapes is required to measure the Doppler line width which is related to k_B. The Doppler width is a result of the velocity distribution of the molecules in the gas cell. To obtain an accurate modelling of the recorded high resolution absorption line-shapes and to measure the Doppler width, we have to take into account different physical effects such as pressure broadening, pressure-induced shifting, and molecular speed dependent effects.

To model the line-shapes of our spectral lines, we have used the SDV model. The spectral line-shape is given by the following function:

$$\alpha(\nu - \nu_0) = S\left(\frac{K(x, y)}{\sigma\sqrt{\pi}}\right), \tag{2}$$

where $S = S_0 PL$ with S_0 being the line strength, P the partial pressure of the gas, and L the absorption path-length. $K(x, y)$ is the spectral line-shape of choice. Our program reads in unit-less parameters x and y that are defined as follows:

$$x = \left(\frac{\nu - \nu_0 - \Delta}{\sigma}\right). \tag{3}$$

In Eq. (3), ν_0 is the angular frequency of the molecular line center, Δ is the collisional shift, and $\sigma = \nu_0\sqrt{\frac{2k_BT}{Mc^2}}$ is the calculated Doppler half width at e^{-1} intensity ($\gamma_D = \sqrt{(ln2)}\sigma$. In this equation, M is the molecular mass of acetylene. The parameter y can be defined as

$$y = \frac{\Gamma}{\sigma}, \tag{4}$$

where Γ is the line width considering all contributions to line broadening.

The collisional broadening and shifting slightly depend on the molecular speed. Taking this dependence into account, the line-shape profile becomes the SDV profile. Following the formalism developed by Berman,[16] Ward,[15] and Pickett,[17] the SDV expression becomes

$$I_{SDV} = \frac{1}{\pi} Re\left[\int_{-\infty}^{+\infty} \frac{f_M(\vec{v})}{(\Gamma(v) - i(\omega - \Delta(v) - \vec{K}.\vec{v})} d^3\vec{v}\right], \tag{5}$$

where $f_M(\vec{v})$ is the Maxwell-Boltzmann distribution of molecular velocities with $\vec{K}$ as the wave vector. By using the Kummer confluent hypergeometric function, $F_1(a, b, z)$, the collisional broadening and shifting could be written as

$$\Gamma(v) = \frac{\Gamma}{2^{m/2}} {}_1F_1\left(-\frac{m}{2}, \frac{3}{2}, -\left(\frac{v}{v_{MPS}}\right)^2\right), \tag{6}$$

$$\Delta(v) = \frac{\Delta}{2^{n/2}} {}_1F_1\left(-\frac{n}{2}, \frac{3}{2}, -\left(\frac{v}{v_{MPS}}\right)^2\right). \tag{7}$$

In Eq. (6) and (7), m and n were parameters related to the intermolecular potential which is approximated by an inverse power form, namely, $V(r) = r^{-q}$ with $m = (q - 3)/(q - 1)$, $n = -3/(q - 1)$. Here, v_{MPS} was the most probable speed of the emitter molecules and it can be obtained using Eq. (8)

$$v_{MPS} = \left(\frac{2k_BT}{M_{C_2H_2}}\right)^{1/2}. \tag{8}$$

Having used the dimensionless parameters x and y which have already been defined, the SDV profile in Eq. (5) can be rewritten to the following form:[16]

$$I_{SDV} = \frac{1}{2\sqrt{\pi}}\left\{1 - \frac{4}{\pi}\int_0^{+\infty} tan^{-1}\left[\frac{x(z)^2 + y(z)^2 - z^2}{2zy(z)}\right] e^{-z^2} z\, dz\right\}, \tag{9}$$

with $z = \frac{v}{v_{MPS}}$ and $tan^{-1} \in [-\pi/2, \pi/2]$. The profile was simulated using MATLAB software. This software program was used to fit the experimental data to the theoretical line-shape.

III. EXPERIMENTAL PROCEDURE

The spectra analysed in this study, have been recorded using a 3-channel tunable diode laser spectrometer designed for line-shape studies of gases. It uses a New Focus Velocity Laser System, tunable between 1500 nm and 1640 nm, and achieving a high signal to noise ratio (>2000), making this instrument quite useful for low pressure studies such as this one.

The instrument setup is presented in Figure 1. The first channel includes a temperature and pressure controlled gas cell. The second channel incorporates a room temperature reference gas cell. Both cells have the same path length of 1.54 m. The third channel records the background signal. Measuring the signals of the three channels simultaneously, we are able to perform an accurate line-shape analysis.

A. Temperature and pressure measurement

To test the thermal stability and thermal gradient inside the cell, we performed several experiments. The temperature controlled absorption gas cell which is centered inside a vacuum jacket, minimizes the thermal conductive/convective coupling to the outside cell. The heating/cooling is supplied by a temperature-controlled fluid that is in direct contact with the cell body to make sure that the temperature gradients are minimized.

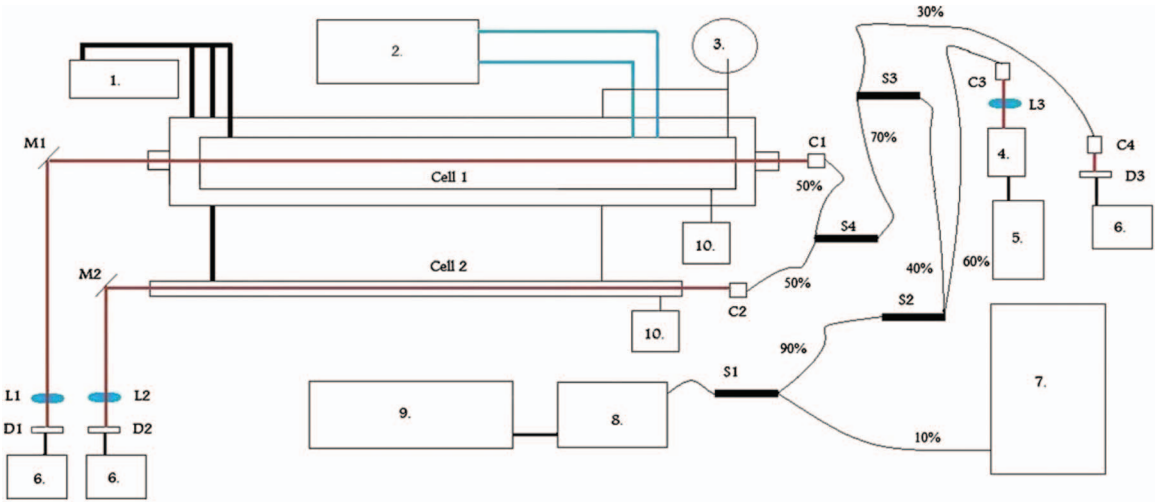

FIG. 1. Spectrometer setup: Legend: 1 – vacuum system; 2 – cooling system NesLab ULT-80 Chiller; 3 – gas sample; 4 and 5 – Fabry Perot interferometer and controller; 6 – detector pre-amplifiers and power supplies; 7 – *WA*-1500 EXFO wavemeter; 8 and 9 – velocity diode laser head and controller; 10 – MKS Baratron pressure gauges; *L*1, *L*2, and *L*3 – focusing lenses; *M*1 and *M*2 – directing mirrors; *D*1, *D*2, and *D*3 – InGas detectors; *C*1−*C*4 – collimators; *S*1−*S*4 – fiber splitters; Vacuum lines are shown in thick black lines. Coolant lines are shown in blue. Laser path is shown by the red lines. Thin curved lines show fiber optic cables.

The main concern in the operation of our variable temperature cell has been the temperature gradient along the length of the cell. Though it is not feasible to remove thermal gradients from the design of absorption cells completely, improvements have been made as solution. Platinum resistor thermometers are mounted on rods in different depths and distances and attached to the cell flanges. We have used multiple temperature sensors to monitor the temperature variability of the cell over its base length. We have calibrated thermometers using the triple point of water.

The diagram of the temperature sensor setup is given in Figure 2. One of the flanges has three temperature ports, one pressure port, and a gas inlet port. The other flange has four temperature ports and one gas outlet port. The heating/cooling of the gas inside the temperature controlled cell is performed using a Neslab ULT-80 thermal bath.

Based on the tests we performed at room temperature, the averaged thermal stability in our gas cell was 0.0052 K over the 4 h of measurement as can be seen in Figure 3. We also checked the vertical and horizontal thermal gradient inside the cell and obtained that larger gradients are formed at the lower temperatures, but at room temperature the thermal horizontal gradient within both ends was 1.6×10^{-4} K/cm. The measured vertical temperature gradient was 4.17×10^{-5} K/cm which is smaller than the horizontal one.

The pressures of the gas samples are monitored using two MKS Baratron capacitance manometers with a full scale reading of 10 Torr (for the temperature controlled gas cell) and 100 Torr (for the reference gas cell) and their accuracy is in order of 10^{-5} Torr. There was only a negligible drift in the overall pressure with time as a result of local temperature instability in the laboratory.

Our pure gas sample of acetylene was supplied by Praxair with a quoted concentration of 99.99%. Using our spectrometer setup, we recorded spectra for *P*(25) transition in the $\nu_1 + \nu_3$ absorption band of C_2H_2 at an average temperature of 295.78 K. For this transition, we recorded spectra at different pressures in the 0.25 Torr–9 Torr range. We recorded the spectra four times for each pressure and we should note

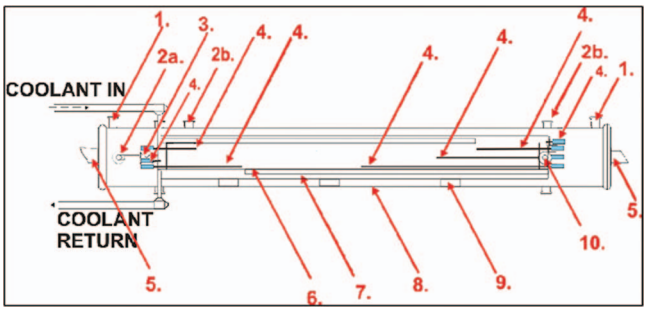

FIG. 2. Side view of the temperature controlled cell. Legend: 1 – vacuum port, 2a – gas inlet, 2b – vacuum field-through for platinum resistors, 3 – vacuum valve, 4 – temperature sensors using platinum resistors, 5 – CaF_2 windows mounted at Brewster angle, 6 – fins for directing the coolant through the coolant jacket, 7 – coolant jacket, 8 – outer cell body, 9 – cell support, 10 – valve for de-pressuring of the outer jacket.

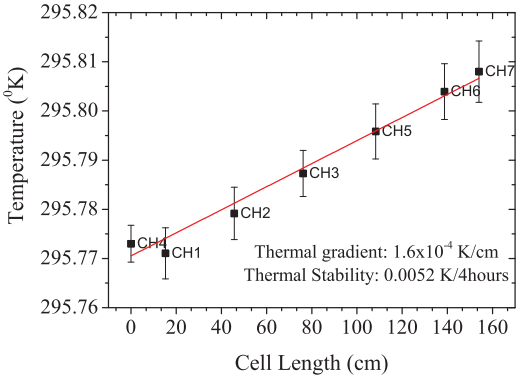

FIG. 3. Thermal gradient and thermal stability for 7 thermometers in the inner cell during 4 h.

that every measurement itself is actually the average of 100 measurements.

IV. SPECTROSCOPIC RESULTS AND ERROR ANALYSIS

We have used LabVIEW software to monitor and record spectra which operates using a New Focus Velocity laser system. The interface of the laser virtual instrument in LabVIEW allows the user to be able either to select the desired wavelength for scanning or to select specific transitions to be scanned. Scanning with our instrument is possible by setting the laser's center wavelength to the preferred starting wavelength. When the center wavelength has been set, we can measure pressure and temperature with our instrument. Then, the piezo voltage is ramped from −3 V up to 2.7 V (which corresponds to a window of just over 30 GHz) in an user set interval usually around 0.001 V. At each step and for each detector, we record the average and standard deviation of 100 points. At the end of the piezo scan we measure pressure and temperature again then take the process for a new central wavelength to be repeated.

Our spectrometer incorporates a Thorlabs SA200-14A Fabry Perot (FP) interferometer to allow for wavelength calibration. The FP cavity offers a 1.5 GHz (0.05 cm^{-1}) free spectral range (FSR) and has a high finesse. Two important aspects in testing the FP cavity were examining the fringe spacing to confirm the FSR of 0.05 cm^{-1}; and then confirming the measurements of line positions. In order to confirm the size of the FSR of the FP cavity, the following experiment was done.

For this test, the laser piezo was scanned from −2 to 2 V in a very slow manner with 3 s between samples. This was done to enable the measurement of 3 wavelengths from the WA1500 EXFO wavemeter. The average and standard deviation of the wavelengths was calculated for each laser piezo voltage recorded. After a complete laser piezo scan had been recorded the wavenumbers associated with each peak were found and subtracted from each other to find the average FSR for that scan. Our results of average spacing for five scans, showed that the free spectral range for the FP cavity is 0.049616 ± 0.000381 cm^{-1}. This result confirms the use of 0.05 cm^{-1} as the correct fringe spacing for any analysis completed with this system. Once the wavelength scale has been determined, a transmission file can be created. We used Chebyshev polynomial functions to correct the background of the spectral files. The frequency is measured directly by using our calibrated EXFO wavemeter.

The nonlinearity of the piezo element has been corrected through the inclusion of a FP interferometer in conjunction with the wavemeter to determine the wavelength of the laser. This method allows us to record reliable wavelength scales. When a scan is completed over multiple FSRs, we record the wavelength of the laser at the first FP peak. Using this wavelength and the properties of the FP cavity we can then determine the wavelength of every other peak recorded by the cavity. For a complete scan of the piezo in the laser, we can observe almost 30 peaks associated with the FSR of the FP cavity. We know from previous observations that the piezo nonlinearity is roughly that of a cubic function. Therefore, these 30 peaks will allow for 29 separate sub-regions where the piezo will appear linear in the local domain between successive peaks.

We also examined the reproducibility of line-width in our measurement. To verify the uncertainty of line-width measurement, we examined 500 identical spectra and determined the uncertainty in the line-width for our spectra. At pressure about 0.5 Torr, the average line-width at half maximum was found to be 0.0098 cm^{-1} with error of 4.13×10^{-7} cm^{-1} for the line center which shows the reproducibility of our recordings.

For the low pressure, we examined spectra of the $\nu_1 + \nu_3$ band. This band was ideal for our experiments because it is a strong absorption band and accurate line positions are available in the literature.[21–23] The dual chamber setup allowed for the simultaneous measurement of line positions inside both the reference cell and the temperature controlled cell. After taking the difference between each of the retrieved line positions, it was found that the line position between the two channels differs by an average of 1.65×10^{-5} cm^{-1} associated with the combination of wavemeter and FP cavity.

The analysis of the recorded spectral files is accomplished by first creating a wavelength scale using the combined information obtained from the wavemeter and the positions of the FP peaks. The transmission profiles were fitted with the SDV line-shape model to obtain the residuals (Observation−Calculation) for each pressure. The software minimizes the differences between the experimental spectra and the calculated spectra by adjusting various line parameters through nonlinear least squares. The improved quality of the residuals indicates a higher accuracy in the line-shape parameters obtained.

In our analysis procedure, we have fitted the line position, intensity, broadening, and Doppler width while fixing the self-shifting values to the highly accurate values determined previously by our group.[23] Figure 4 shows the spectra of the $P(25)$ line fitted with the SDV model measured at 295.78 K and at different pressures. The upper panel shows the observed data and the lower panel shows the residuals plotted for several pressures. Each of the lower panels was plotted with the same vertical scale to make it easier to compare them.

Figure 4 presents the results of fitting our spectral profile in the pressure range of 0.25–5 Torr using the SDV profile. In the implementation of the SDV profile, the broadening and shift are assumed to depend on collisional speed, and on inverse power law expression for the inter-molecular potential energy surface. We performed fits with different values of the q parameter and found that the residuals are minimized for $q = 5$, in agreement with the findings of Hashemi *et al.*[24] As it is clear from an examination of our fit residuals, the SDV line-shape model reproduces the experimental spectra with good accuracy.

The bottom panel in Figure 4 shows that at lower pressures, SDV profile is considered to simulate well the recorded spectra with the noise level. We can also see the "*W*" shape structure in the center of the residuals specially in pressures above 1 Torr. To interpret this effect, we should mention that the collisions induce a confinement of molecules by the surrounding molecules which can cause the Doppler

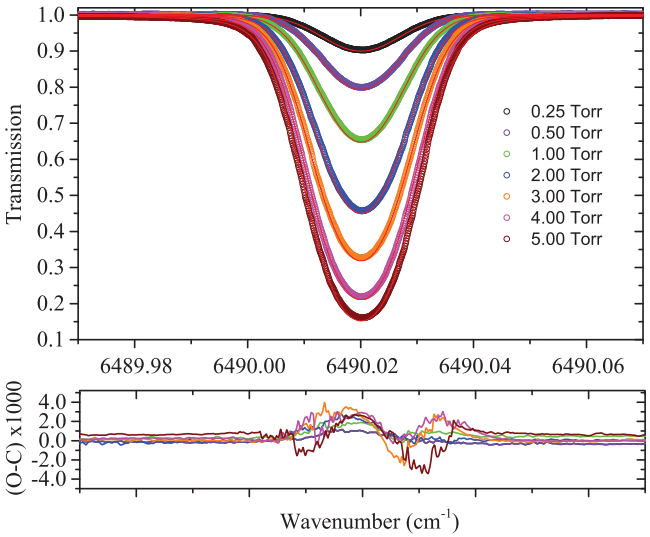

FIG. 4. Sample plot of the transmission spectrum of the $P(25)$ line of C_2H_2 at pressures 0.25–5 Torr and 295.78 K. Residuals $(O - C)$ under these conditions resulting from least squares single-spectrum fittings of experimental data to SDV line-shape model (bottom panels).

contribution of the line shape become narrower.[12] Considering SDV profile, we cannot fit for narrowing parameter. To take into account this parameter besides speed dependent effects, we need to do the simulations of spectra with line-shape models that take into account the narrowing effects, such as the pCSDHC model.[20]

In the fitting procedure, both the self-broadening (γ_S) and Doppler broadening (γ_D) are related to the width of the line. Thus, they cannot be fitted simultaneously as they are highly correlated. To determine a precise value for γ_S, we first calculated the standard deviation of all γ_D values across all pressures for γ_S values and plotted the results. We then fitted these points to a quadratic function and calculated the minimum based on the first derivative of the equation of best fit. The minimum value we obtained served to be our optimum γ_S value. For the obtained γ_S value, we fitted for γ_D and obtained a pressure dependence relationship for γ_D.

Hence, the Doppler width values can be plotted as a function of the gas pressure and, by doing a fit to a linear function, one can take the zero-order coefficient with its statistical uncertainty as zero-pressure measurement of the Doppler width. This would lead to the correct evaluation of the statistical uncertainty. We found that the zero-order width is equal to 0.00125 cm^{-1} with error about 6.12×10^{-6} cm^{-1}.

The γ_D values were plotted in a diagram with the pressure in one axis. The γ_D value should be constant with pressure as it is only a function of physical constants. Therefore, the correct γ_S coefficient should allow for the retrieval of a constant, γ_D. This can be seen in Figure 5 where γ_D remains constant as the pressure changes. After finding the ideal value for the self-broadening coefficient, we were able to refit our data and obtain new values for the γ_D. For example, for the self-broadening value equal to 0.107 cm^{-1} atm^{-1} we obtained the averaged $\gamma_D = 0.0012507$ cm^{-1} with a statistical error of 1.066×10^{-8} cm^{-1}.

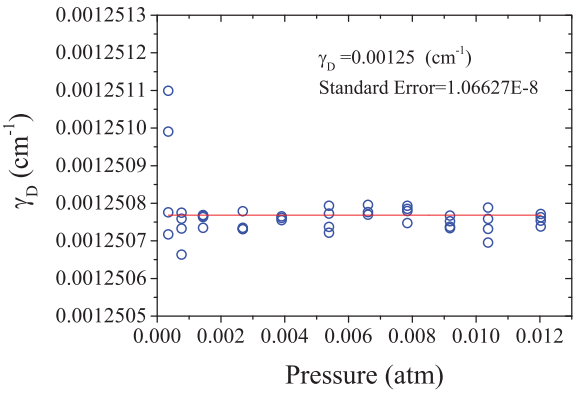

FIG. 5. Plot of Doppler broadening values were remained constant across all pressures; the averaged value of Doppler width and the standard error is shown in this diagram.

To calculate Doppler width values and their errors at different pressures, we first performed different fits for recorded data at different pressures and obtained Doppler width values together with their errors. Then, we obtained k_B for each of the Doppler width values and found the mean value for k_B as shown in Figure 6. In this procedure, 44 spectra was used. Using these γ_D values, we were able to calculate k_B using Eq. (1) to obtain the accurate values for k_B. We obtained that in the low pressure the average value of k_B is 1.38066×10^{-23} J K^{-1} for SDV model.

A. Statistical and systematic error analysis

Determining an accurate value for k_B requires better knowledge of different error sources. Considering Eq. (1), the uncertainty of our calculation for k_B is due to the uncertainties in measuring ν, T, and γ_D as can be seen in Eq. (10). Moreover, we should take into account the error resulted from line-shape model we used. The following expression is used to determine the error in k_B:

$$\frac{\delta_{k_B}}{k_B} = \sqrt{4\left(\frac{\delta_{\gamma_D}}{\gamma_D}\right)^2 + 4\left(\frac{\delta_\nu}{\nu}\right)^2 + \left(\frac{\delta_T}{T}\right)^2}. \qquad (10)$$

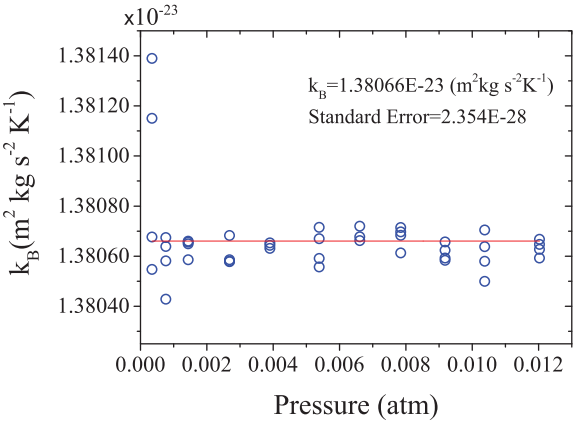

FIG. 6. Plot of calculated Boltzmann constant values within its mean value and standard error across pressure.

In order to identify the type A error in temperature, the standard deviation of the mean for temperature was calculated to be 0.005 K. We tested the temperature stability of our inner cell by recording data each 60 s over a time span of about 4 h. The relative error contribution of temperature stability was 1.75×10^{-5}. Also, we considered the error due to the temperature horizontal gradient and we obtained that the relative uncertainty was 8.33×10^{-5} for the whole inner chamber. Investigating the temperature vertical gradient resulted in relative error contribution to be 0.00014×10^{-5} which is smaller compared to the horizontal error along the cell. Therefore, the relative error due to the temperature measurement was 8.51×10^{-5}. The statistical errors of the line positions were determined similarly.

The relative uncertainties for the Doppler width (γ_D), position (ν), and temperature (T) which are the most important error contributors were found to be 0.84×10^{-5}, 0.00038×10^{-5}, and 8.51×10^{-5} for the average calculation, respectively. Line-center frequency measurement showed that the relative error is 0.00025×10^{-5}.

It is clear from these error results that the largest contribution to error is obtained from the temperature measurement within this experiment. Using these values the resulting relative error for k_B is 8.54×10^{-5} for SDV model.

Taking into account the different error budgets, we also calculated the systematic error in our measurement. First of all, the combined uncertainty of the temperature measurement and the resistance or voltage measurement can be expressed as an equivalent temperature uncertainty in millikelvin (mK). The uncertainty varies with temperature due to the variation of the sensor sensitivity and excitation. When a sensor is used to measure temperature, a polynomial fit to the measured calibration data is often used to convert the sensor resistance (R) or voltage (V) to a temperature (T). How well the polynomial represents the sensor calibration data is another source of uncertainty when using the sensor. The absolute error was found to be 2.4 mK as our systematic source of temperature measuring and leads the relative error contribution of 0.81×10^{-5}.

The error of frequency scale measurement that comes from frequency calibration from FP interferometer and EXFO wavemeter was in order of 10^{-5} cm^{-1}. The wavemeter precision is in order of 10^{-3} cm^{-1}, but our calibration processes offer an error in line position on the order of 10^{-5} cm^{-1} using the FP cavity, the wavemeter, and channel 2 spectra, gives rise to 1.65×10^{-5} cm^{-1} error in the wavenumber (as it is explained in Sec. IV).

Furthermore, in fitting with SDV profile, we have considered the influence of the type of interaction potential in our analysis. Using $q = 5$ resulted in less error in simulation of the spectra and its average relative error calculated to be 0.38×10^{-5}.

Based on all these error budgets the relative error of k_B is 1.87×10^{-5} which is smaller than the statistical error we obtained. Combining both types of error, our global error in calculation of k_B is 8.74×10^{-5}. This error in our measurement is less than the errors reported in the findings of the previous studies by Casa *et al.*[3] and Djerroud *et al.*[5] where they have obtained this uncertainty to be 1.6×10^{-4} and 1.9×10^{-4}, respectively, and it is four times larger than the obtained result by Castrillo *et al.*[14] where they have obtained the relative uncertainty to be 2.4×10^{-5}.

V. CONCLUSIONS

In this study, we have performed a line-shape analysis of acetylene at room temperature and low gas pressures. Accurate line-shape parameters have been obtained considering Speed Dependent Voigt profile. The calculated value for the Boltzmann constant using Doppler thermometry in our experiment was 1.38066×10^{-23} J K^{-1} with relative statistical uncertainty of 8.54×10^{-5} at low pressure for SDV model. Also, the relative systematic error in for k_B was 1.87×10^{-5}.

We can conclude that our limiting factor was not the signal to noise ratio but the line-shape model used and the determination of the line-shape parameters. Using error analysis, most of the uncertainty in this measurement was due to the temperature measurement and next due to line-shape model that was used. For our temperature measurements, the thermal gradient was the largest error contributor.

The uncertainty in the modelling of collisional effects was limited by our knowledge on the fitting parameters such as self-broadening, Doppler width, and parameter q and thus parameters m and n in the SDV model.

ACKNOWLEDGMENTS

This work was supported by the Natural Sciences and Engineering Research Council of Canada through the Discovery and CREATE programs. We would like to further thank the AMETHYST program at the University of Lethbridge for their continued funding and academic support.

[1] P. J. Mohr, B. N. Taylor, and D. B. Newell, Rev. Mod. Phys. **84**, 1527 (2012).
[2] C. Daussy, M. Guinet, A. Amy-Klein, K. Djerroud, Y. Hermier, S. Briaudeau, C. J. Bordé, and C. Chardonnet, Phys. Rev. Lett. **98**, 250801 (2007).
[3] G. Casa, A. Castrillo, G. Galzerano, R. Wehr, A. Merlone, D. Di Serafino, P. Laporta, and L. Gianfrani, Phys. Rev. Lett. **100**, 200801 (2008).
[4] K. M. Yamada, A. Onae, F.-L. Hong, H. Inaba, and T. Shimizu, C. R. Phys. **10**, 907 (2009).
[5] K. Djerroud, C. Lemarchand, A. Gauguet, C. Daussy, S. Briaudeau, B. Darquié, O. Lopez, A. Amy-Klein, C. Chardonnet, and C. J. Bordé, C. R. Phys. **10**, 883 (2009).
[6] L. Moretti, A. Castrillo, E. Fasci, M. D. De Vizia, G. Casa, G. Galzerano, A. Merlone, P. Laporta, and L. Gianfrani, Phys. Rev. Lett. **111**, 907 (2013).
[7] C. Lemarchand, M. Triki, B. Darquié, C. J. Bordé, C. Chardonnet, and C. Daussy, New J. Phys. **13**, 073028 (2011).
[8] C. Lemarchand, S. Mejri, P. L. T. Sow, M. Triki, S. K. Tokunaga, S. Briaudeau, C. Chardonnet, B. Darquie, and C. Daussy, Metrologia **50**, 623 (2013).
[9] G.-W. Truong, E. F. May, T. M. Stace, and A. N. Luiten, Phys. Rev. A **83**, 033805 (2011).
[10] A. Cygan, D. Lisak, R. Trawiński, and R. Ciuryło, Phys. Rev. A **82**, 032515 (2010).
[11] W. Voigt, Sitzber. Bayr Akad. München Ber. **1912**, 603 (1912).
[12] R. Dicke, Phys. Rev. **89**, 472 (1953).
[13] L. Galatry, Phys. Rev. **122**, 1218 (1961).
[14] A. Castrillo, L. Moretti, E. Fasci, M. D. Vizia, G. Casa, and L. Gianfrani, J. Mol. Spectrosc. **300**, 131–138 (2014).
[15] J. Ward, J. Cooper, and E. W. Smith, J. Quant. Spectrosc. Radiat. Transfer **14**, 555 (1974).
[16] P. R. Berman, J. Quant. Spectrosc. Radiat. Transfer **12**, 1331 (1972).

[17]H. Pickett, J. Chem. Phys. **73**, 6090 (1980).
[18]A. Pine, J. Chem. Phys. **101**, 3444 (1994).
[19]A. Pine, J. Quant. Spectrosc. Radiat. Transfer **62**, 397 (1999).
[20]H. Tran, N. Ngo, and J.-M. Hartmann, J. Quant. Spectrosc. Radiat. Transfer **129**, 199 (2013).
[21]A. A. Madej, A. J. Alcock, A. Czajkowski, J. E. Bernard, and S. Chepurov, J. Opt. Soc. Am. B **23**, 2200 (2006).
[22]L. Rothman, I. Gordon, Y. Babikov, A. Barbe, D. Chris Benner, P. Bernath, M. Birk, L. Bizzocchi, V. Boudon, L. Brown *et al.*, J. Quant. Spectrosc. Radiat. Transfer **130**, 4 (2013).
[23]C. Povey, A. Predoi-Cross, and D. R. Hurtmans, J. Mol. Spectrosc. **268**, 177 (2011).
[24]R. Hashemi, H. Rozario, C. Povey, and A. Predoi-Cross, J. Quant. Spectrosc. Radiat. Transfer **140**, 58 (2014).